JACS
JOURNAL OF THE AMERICAN CHEMICAL SOCIETY
Article
pubs.acs.org/JACS

Insights into the Mechanism of Tandem Alkene Hydroformylation over a Nanostructured Catalyst with Multiple Interfaces

Ji Su,[†,⊥] Chenlu Xie,[‡,⊥] Chen Chen,[‡,∥,⊥] Yi Yu,[‡] Griffin Kennedy,[†,‡] Gabor A. Somorjai,*[,†,‡] and Peidong Yang*[,†,‡,§]

[†]Materials Sciences Division, Lawrence Berkeley National Laboratory, Berkeley, California 94720, United States
[‡]Department of Chemistry, University of California, Berkeley, California 94720, United States
[§]Kavli Energy Nanosciences Institute, Berkeley, California 94720, United States

Supporting Information

ABSTRACT: The concept of tandem catalysis, where sequential reactions catalyzed by different interfaces in single nanostructure give desirable product selectively, has previously been applied effectively in the production of propanal from methanol (via carbon monoxide and hydrogen) and ethylene via tandem hydroformylation. However, the underlying mechanism leading to enhanced product selectivity has remained elusive due to the lack of stable, well-defined catalyst suitable for in-depth comprehensive study. Accordingly, we present the design and synthesis of a three-dimensional (3D) catalyst CeO_2−Pt@mSiO_2 with well-defined metal−oxide interfaces and stable architecture and investigate the selective conversion of ethylene to propanal via tandem hydroformylation. The effective production of aldehyde through the tandem hydroformylation was also observed on propylene and 1-butene. A thorough study of the CeO_2−Pt@mSiO_2 under different reaction and control conditions reveals that the ethylene present for the hydroformylation step slows down initial methanol decomposition, preventing the accumulation of hydrogen (H_2) and favoring propanal formation to achieve up to 80% selectivity. The selectivity is also promoted by the fact that the reaction intermediates produced from methanol decomposition are poised to directly undergo hydroformylation upon migration from one catalytic interface to another. This synergistic effect between the two sequential reactions and the corresponding altered reaction pathway, compared to the single-step reaction, constitute the key advantages of this tandem catalysis. Ultimately, this in-depth study unravels the principles of tandem catalysis related to hydroformylation and represents a key step toward the rational design of new heterogeneous catalysts.

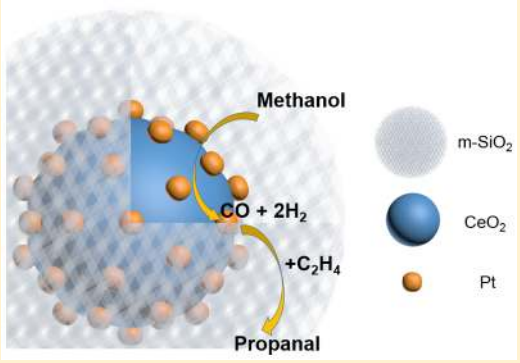

1. INTRODUCTION

Nanocrystalline inorganic catalysts for heterogeneous reactions have recently been the subject of extensive research due to their essential role in modern chemical industrial processes.[1−3] Thus far, the design and development of these catalysts has been exclusively carried out at the single-interface length scale, where the atomic arrangements on the catalytic interface are tuned to alter the activity and selectivity of a single chemical conversion process.[4−8] Recently, however, tandem catalysis was demonstrated in a heterogeneous gas-phase reaction,[9] wherein two metal−oxide interfaces in a single nanostructure catalyzed sequential chemical conversions with high product selectivity. This work has inspired us to explore the rational design of nanocrystalline heterogeneous catalysts beyond the single interface length scale. Specifically, instead of optimizing a single catalytic interface, the tandem catalyst design takes advantage of the synergy between different chemical conversions on multiple spatially arranged interfaces to achieve desirable product distributions. In this context, harmonized reaction kinetics at two interfaces can facilitate the overall sequential reactivity wherein one reactive species modulates the chemical conversion of another. Thus, a thorough study of heterogeneous tandem reactions, which is yet to be carried out, would help to elucidate the underlying principles of such catalysis and open up new opportunities for application in heterogeneous reactions.

A model system for tandem catalysis is the ethylene hydroformylation reaction, where the first chemical conversion is the production of hydrogen (H_2) and carbon monoxide (CO) by methanol decomposition, followed by ethylene hydroformylation. This reaction is ideal not only because the production of aldehydes via alkene hydroformylation is an essential industrial process[10,11] but also due to the fact that the initial decomposition of methanol and subsequent hydroformylation are chemically orthogonal and compatible reactions. Previous research on alkene hydroformylation via heterogeneous catalysis led to the development of nanocrystal-

Received: April 15, 2016
Published: September 2, 2016

DOI: 10.1021/jacs.6b03915
J. Am. Chem. Soc. 2016, 138, 11568−11574

line Rh- and Pt-based catalysts.[12−16] However, these catalysts gave low aldehyde selectivity due to dominance of the competing alkene hydrogenation reaction.[17−19] We previously showed that tandem catalysis is a plausible approach to overcome this low selectivity, where propanal could be preferentially produced by reacting ethylene with H_2 and CO formed in situ over a nanocrystal bilayer CeO_2−Pt−SiO_2.[9] The origin of the high selectivity has yet to be elucidated, however, and an in-depth study of this tandem reaction would bring new insights concerning tandem catalysis.

An essential prerequisite for successful implementation of tandem catalysis is the synthesis of the complex nanostructured catalyst. Although the drop-casted bilayer CeO_2−Pt−SiO_2 catalyst was adequate to demonstrate tandem catalysis, it exhibited poor stability toward aggregation and low active site density.[20,21] In order to thoroughly study the tandem hydroformylation reaction and gain insights into the fundamental principles behind this sort of catalysis, a stable, well-defined catalyst is necessary. Such a catalyst could be obtained by engineering both catalytic interfaces into one particle. Enclosing this particle in mesoporous silica ($mSiO_2$) would further provide thermal stability and enhance active-site accessibility by favoring the high surface area, powdered form of the catalyst.[17,21] Fundamentally, the fabrication of such a complex nanostructure is of synthetic significance and would be a great example of utilizing the synthetic control of inorganic nanocrystals to pursue the next generation heterogeneous catalysts.

Herein, we report the design and synthesis of a new generation tandem catalyst, the three-dimensional CeO_2−Pt@$mSiO_2$, with a core−shell configuration that consists of a CeO_2−Pt core and mesoporous silica shell. Tandem hydroformylation reactions carried out by this 3D catalyst show greatly enhanced propanal selectivity compared to the single-step ethylene hydroformylation with CO and H_2. Significantly, the catalytic tandem hydroformylation can also be extended to propylene and 1-butene. Further study of the tandem hydroformylation indicates that the superior propanal selectivity can be attributed to the synergy between the two sequential reactions and the altered reaction pathway afforded by the tandem reaction compared to the single-step reaction.

2. RESULTS AND DISCUSSION

2.1. Synthesis and Characterizations of 3D Tandem Catalysts. The CeO_2−Pt@$mSiO_2$ catalyst consists of a CeO_2−Pt core and mesoporous silica shell and thus features both Pt/CeO_2 and Pt/SiO_2 functional interfaces. Importantly, while Pt/CeO_2 is a typical catalytic interface for methanol decomposition to produce CO and H_2,[22,23] Pt/SiO_2 has been shown to exhibit catalytic activity for the hydroformylation of ethylene with CO and H_2.[12] Thus, with these integrated interfaces, this catalyst could convert methanol and ethylene to propanal through a tandem process. Indeed, methanol could diffuse through the mesoporous silica shell to the Pt/CeO_2 core, whereby it would be decomposed to CO and H_2. The subsequent outward diffusion of the CO an H_2 through the $mSiO_2$ channels and reaction with ethylene would then result in the formation of propanal at the nearby Pt/SiO_2 interface, completing the two-step reaction.

The synthesis of the CeO_2−Pt@$mSiO_2$ was carried out over the course of three steps (Figure 1). Well-dispersed and uniform CeO_2 nanoparticles were first synthesized via a solvothermal method, and subsequently, Pt nanocrystals were grown directly on the CeO_2 surface.[19] Finally, the CeO_2−Pt nanocrystal were coated with mesoporous silica and annealed in air to obtain CeO_2−Pt@$mSiO_2$.[21,24] The as-synthesized nanoparticle was characterized by transmission electron microscopy (TEM) and energy-dispersive X-ray spectroscopy (EDS), which clearly showed its complex core−shell structure (Figure 1 and Figure 2). The Pt loading was further calculated to be 5.14% from inductively coupled plasma atomic emission spectroscopy (ICP-AES) (Table S1). The porosity of CeO_2−Pt@$mSiO_2$ was confirmed by nitrogen physisorption, while the pore size distribution curve calculated from the adsorption branch of the isotherms exhibited a maximum at 2.4 nm. The Brunauer−Emmett−Teller surface area of CeO_2−Pt@$mSiO_2$ was calculated to be 236 m^2 g^{-1}, indicating the highly mesoporous nature of the silica shell (Figure S2). Importantly, the 3D nature of CeO_2−Pt@$mSiO_2$ imparts a higher surface area than would be accessible in a bilayer catalyst. Finally, the CeO_2−Pt core maintained its original shape after annealing at

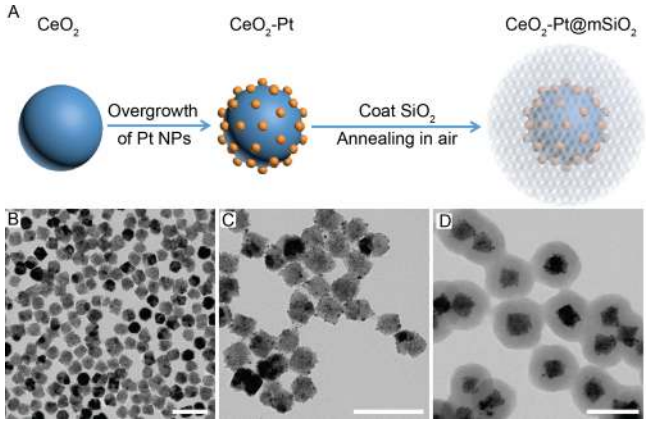

Figure 1. Synthesis and characterization of the 3D nanocrystal tandem catalyst CeO_2−Pt@$mSiO_2$. (A) Synthesis of the tandem catalyst. (B) TEM image of well-dispersed CeO_2 nanoparticles. (C) TEM image of CeO_2−Pt nanoparticles synthesized the overgrowth of Pt. (D) TEM image of core−shell CeO_2−Pt@$mSiO_2$ nanoparticles. Scale bar: 100 nm.

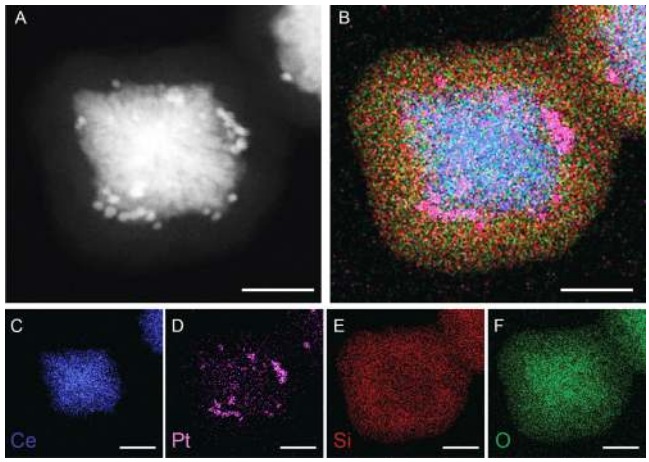

Figure 2. (A) Imaging of CeO_2−Pt@$mSiO_2$ via high-angle annular dark-field scanning transmission electron microscopy. (B) Elemental mapping of CeO_2−Pt@$mSiO_2$ with energy dispersive X-ray spectroscopy (EDS). Corresponding EDS elemental mapping for (C) Ce, (D) Pt, (E) Si, and (F) O, respectively. Scale bar: 30 nm.

DOI: 10.1021/jacs.6b03915
J. Am. Chem. Soc. 2016, 138, 11568−11574

350 °C to remove organic capping ligands and generate a clean interface (see TEM images, Figure S3). Thus, CeO_2−Pt@$mSiO_2$ clearly possesses high thermal stability imparted by the mesoporous SiO_2 shell.

2.2. Catalytic Performance of CeO_2−Pt@$mSiO_2$ in the Hydroformylation of Ethylene with Methanol. *2.2.1. Catalytic Performance of Individual Interfaces in CeO_2−Pt@$mSiO_2$: Tandem Reaction Is Sequentially Catalyzed.* Prior to examining the tandem reaction facilitated by CeO_2−Pt@$mSiO_2$, control experiments were performed to understand the role of each interface in catalysis. Accordingly, the tandem hydroformylation of ethylene with methanol was carried out at 150 °C over the two single interface catalysts CeO_2−Pt and Pt@$mSiO_2$ (Figure 3, Figure S4). The CeO_2−Pt catalyst

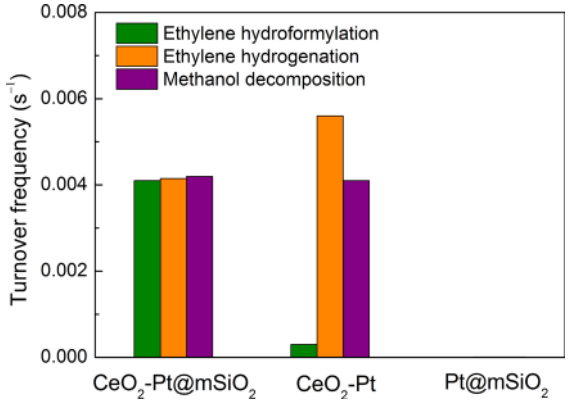

Figure 3. Ethylene hydroformylation with methanol carried out at 150 °C over CeO_2−Pt@$mSiO_2$ and single interface catalysts CeO_2−Pt and Pt@$mSiO_2$. Methanol, ethylene, and helium partial pressures were 35, 7.5, and 727.5 Torr, respectively.

exhibited obvious activity for methanol decomposition, with a turnover frequency (TOF) of 4.2×10^{-3} s^{-1} per Pt atom. However, this catalyst exhibited a very low activity for ethylene hydroformylation to propanal and instead was highly active for ethylene hydrogenation to ethane. The Pt@$mSiO_2$ catalyst showed almost no activity for the tandem hydroformylation due to the fact it is not catalytically active for methanol decomposition, which is the first step of the tandem process (Figure S5). Gratifyingly, a much higher activity for propanal formation was achieved by integrating the Pt/CeO_2 and Pt/SiO_2 interfaces into a tandem catalyst. Indeed, the TOF for ethylene hydroformylation by CeO_2−Pt@$mSiO_2$ was determined to be 4.1×10^{-3} s^{-1} per Pt atom, which is about 13 times greater than the TOF exhibited by CeO_2−Pt alone (3.0×10^{-4} s^{-1} per Pt atom). This significant enhancement in the hydroformylation activity with CeO_2−Pt@$mSiO_2$ clearly demonstrates that the designed interfaces in the tandem catalyst can be used to carry out sequential chemical reactions effectively and selectively.

2.2.2. Comparison of Single-Step Hydroformylation and Tandem Reaction: Synergy between the Sequential Reactions. The production of propanal via sequential chemical conversions at two different neighboring metal-oxide interfaces in CeO_2−Pt@$mSiO_2$ illustrates the unique advantage of the tandem catalysis. In order to unravel the underlying mechanism of propanal formation, we further studied the "decoupled" single-step hydroformylation reaction as a control experiment, wherein ethylene was directly reacted with CO and H_2 present in stoichiometry equal to one equivalent of methanol.

The single-step ethylene hydroformylation and the tandem hydroformylation were examined over CeO_2−Pt@$mSiO_2$ for a range of temperatures from 150 to 230 °C (Figure 4). As shown in Figure 4A, the selectivity for propanal formation in the tandem reaction was much higher than for the single-step hydroformylation for all temperatures. The highest selectivity achieved with tandem hydroformylation was an impressive ~50% at 150 °C compared to only 2.2% for the single-step hydroformylation with CO and H_2. Also considering that ethylene hydrogenation is much more favorable than the ethylene hydroformylation on conventional Pt catalysts,[17,19] intuitively ethane should almost always be the dominant product in this reaction. Thus, the effective and highly selective production of propanal with CeO_2−Pt@$mSiO_2$ suggests an important synergy between the two sequential reactions facilitated with this catalyst.

To gain more insights into this synergistic effect, we examined the temperature dependence of the reaction with in situ methanol decomposition and found that the selectivity for propanal formation decreased with increasing temperature. At 150 °C, the rates of methanol decomposition, ethylene hydroformylation, and ethylene hydrogenation in the tandem process were found to be identical, suggesting that all the CO and H_2 formed in situ from methanol decomposition (1:2 CO to H_2 ratio) was simultaneously and fully consumed by reacting with ethylene, which yields propanal at 50% selectivity without accumulating H_2 and CO on the Pt surface. With elevated

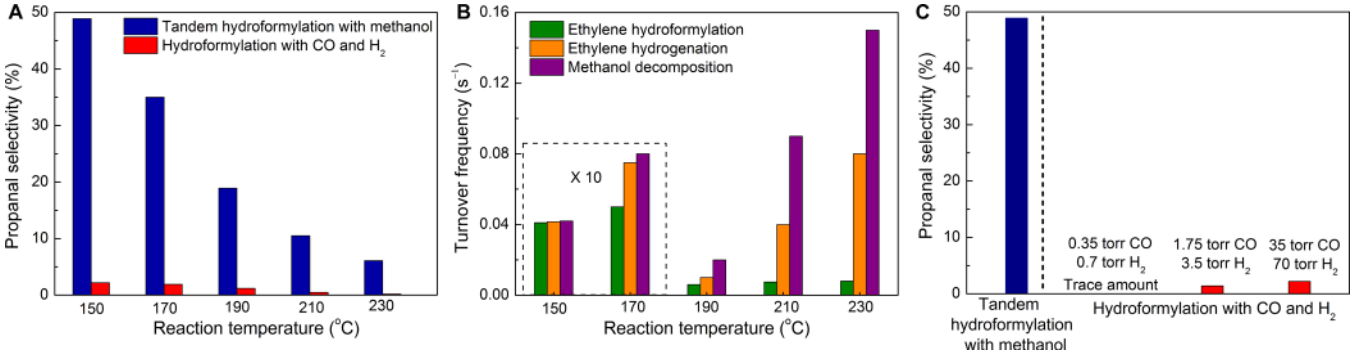

Figure 4. Catalytic performance of CeO_2−Pt@$mSiO_2$ for the hydroformylation of ethylene with methanol at an ethylene pressure of 7.5 Torr. (A) Comparison of tandem hydroformylation of ethylene with methanol and single-step hydroformylation with CO and H_2. (B) The influence of temperature on tandem hydroformylation of ethylene. (C) Catalytic performance of single-step hydroformylation under a deficiency of CO and H_2 at 150 °C.

DOI: 10.1021/jacs.6b03915
J. Am. Chem. Soc. 2016, 138, 11568−11574

temperatures, all three reactions proceeded more rapidly with relative rates as follows: methanol decomposition > ethylene hydrogenation > hydroformylation. Consequently, the selectivity for propanal declined because the rate of ethylene hydrogenation was higher than the hydroformylation and also due to an accumulation of H_2 that disfavored the production of propanal. These results suggest that when the methanol decomposition, and thus H_2 gas accumulation, greatly exceeds ethylene hydroformylation, the selectivity of hydroformylation drops significantly. In other words, a slower methanol decomposition rate favors propanal production and imparts selectivity.

Notably, the high selectivity toward propanal could not be obtained in the single-step hydroformylation even upon artificially creating a deficiency of CO and H_2 to simulate the tandem conditions. When a very small amount of CO and H_2 (equivalent to the stoichiometric amount of actual converted methanol in the tandem process) was introduced to the catalyst with ethylene, ethane was the only product and the formation of propanal was less than the detection limit (<0.01%) (Figure 4C and Table S2). This result led us to consider possible molecular-level mechanisms behind the tandem process, which is likely distinct from the single-step hydroformylation. In the case of tandem reaction, the methanol could decompose to form intermediates H* and CHO* on the Pt/CeO_2 interface,[23,25] which would be adsorbed on the platinum surface and diffuse to the nearby Pt/SiO_2 interface. At this interface, the intermediates would then be fully consumed in the ethylene hydroformylation and hydrogenation reactions, yielding the observed 50% propanal selectivity. Thus, we can conclude that the absence of H_2 accumulation on the Pt surface is the key to the effective formation of propanal, which could be achieved by slow methanol decomposition and the subsequent consumption of CO and H_2 by ethylene in the tandem process.

2.2.3. Effect of Ethylene on Methanol Decomposition: Another Aspect of the Synergy and a Pathway toward Higher Selectivity. We also investigated the influence of ethylene on the methanol decomposition and subsequent hydroformylation. Notably, for all temperatures investigated, we found that methanol decomposition was impeded by the presence of ethylene (Figure 5). For instance, at 150 °C the TOF for methanol decomposition in the absence of ethylene was found to be ~0.49 s^{-1} per Pt atom (Figure S5). Upon introduction of ethylene, however, this TOF decreased significantly and reached a minimum of 4.2×10^{-3} s^{-1} per Pt atom when the ratio of ethylene to methanol was 0.21. Further addition of ethylene to achieve ethylene:methanol ratios >0.21 had no effect on the methanol decomposition rate.

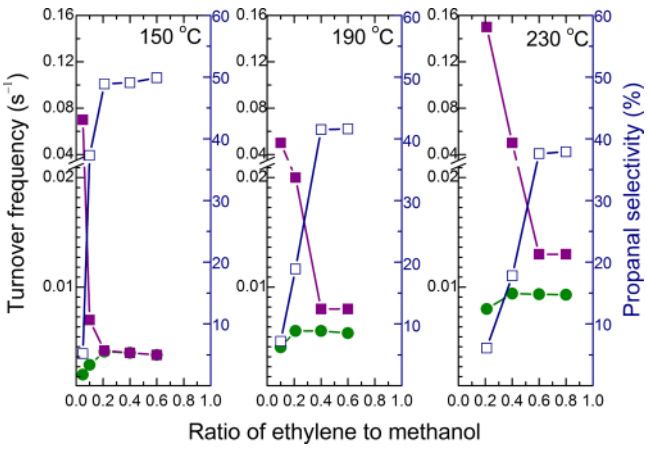

Figure 5. Inhibiting effect of ethylene on methanol decomposition over the CeO_2−Pt@$mSiO_2$ catalyst: changes in methanol decomposition rate (purple ■), ethylene hydroformylation rate (green ●), and propanol selectivity (blue □). Methanol partial pressure was 35 Torr, and the reaction temperature was 150 °C.

We attributed this inhibiting effect to the adsorption of ethylene on the Pt surface and corresponding blockage of the active sites for methanol decomposition. To test this possibility, H_2 gas was cofed to the catalyst with methanol and ethylene (Figure 6, panels A and C), which resulted in a significant increase in the TOF for methanol decomposition. Indeed, the excess H_2 reacted with adsorbed ethylene thereby opening up active sites and enhancing the methanol decomposition rate. This data further supports the observation that variations in the selectivity and TOF for the ethylene hydrogenation and hydroformylation reactions can be attributed to accumulation of H_2, from externally added and the accelerated decomposition of methanol. The presence of ethylene conversely slows this decomposition, and upon achieving an ethylene:methanol ratio > 0.21, the TOF for ethylene hydroformylation becomes identical with methanol decomposition, yielding the propanal selectivity of 50%.

A similar inhibiting effect due to ethylene was observed for temperatures above 150 °C (Figure 5), and notably the rate of ethylene hydroformylation was significantly enhanced at these higher temperatures. For instance, the hydroformylation TOF reached a maximum of 9.4×10^{-3} s^{-1} per Pt atom at 230 °C, more than double the TOF achieved at 150 °C for the same ethylene: methanol ratio. Because methanol decomposition was accelerated at higher temperatures, however, a larger ethylene-to-methanol ratio was necessary to achieve the maximum selectivity for propanal when compared with the lower temperature data. For instance, at 230 °C the ethylene hydroformylation reached its maximum activity and selectivity for an ethylene:methanol ratio of 0.4, compared with the maximum ratio of 0.21 necessary at 150 °C. This observed reactivity with ethylene thus stands as further support of the dual reaction synergy achieved with CeO_2−Pt@$mSiO_2$ catalysis.

Given this comprehensive understanding of the tandem hydroformylation, it is possible to tune the reaction conditions to further increase the selectivity for propanal and the reaction rate simultaneously. As hydroformylation involves CO, ethylene, and H_2, increasing the partial pressure of CO facilitates hydroformylation to compete favorably with hydrogenation and gives higher aldehyde selectivity. As illustrated in Figure 6 (panels B and D), an initial increase in fed CO results in significant enhancement of the TOFs for methanol decomposition and ethylene hydroformylation, whereas the reaction rate of ethylene hydrogenation correspondingly decreased. Upon cofeeding with 70 Torr of CO, the TOF for ethylene hydroformylation increased by a factor of 3 and notably a selectivity as high as 80% could be achieved.

Gratifyingly, we also found that the catalytic tandem hydroformylation reaction was also applicable to other light olefin systems. When propylene or 1-butene were fed over the CeO_2−Pt@$mSiO_2$ catalyst instead of ethylene, hydroformylation occurred to produce butyl aldehyde or pentanaldehyde (Table 1, Table S4). In both cases, the tandem reaction gave much better selectivity compared to the single-step hydro-

DOI: 10.1021/jacs.6b03915
J. Am. Chem. Soc. 2016, 138, 11568−11574

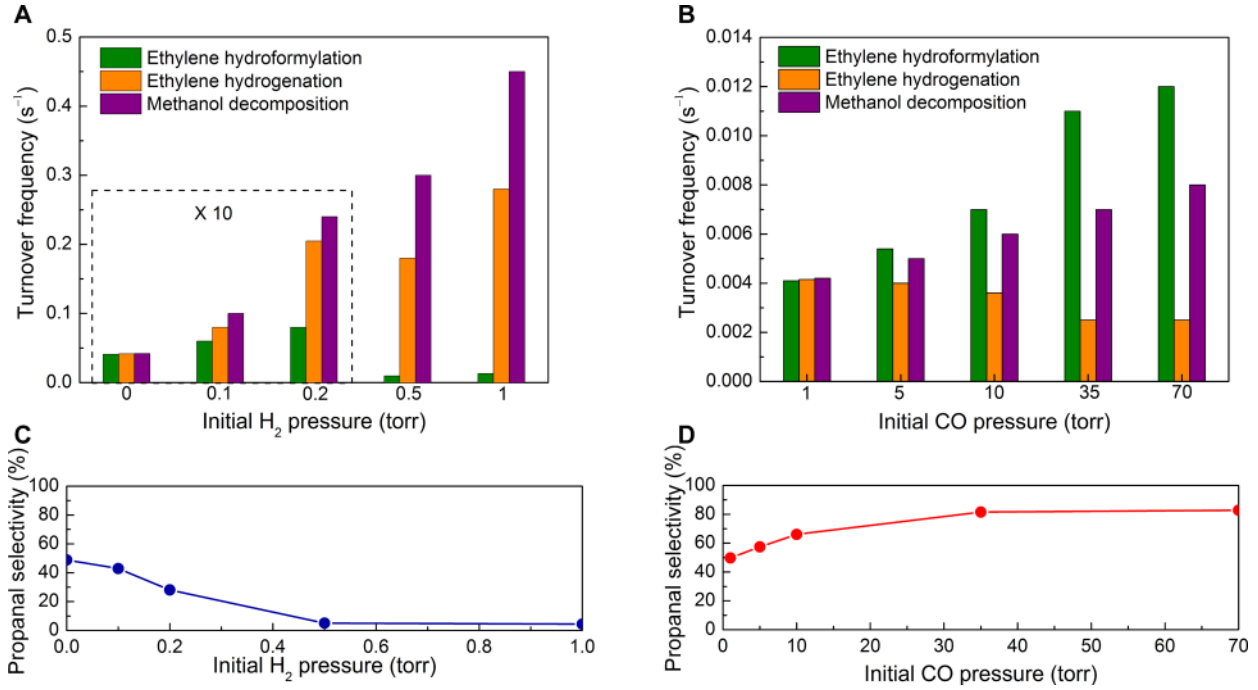

Figure 6. (Top) The effect of cofeeding H_2 or CO on the tandem hydroformylation of ethylene. (A) Cofeeding with H_2 and (B) cofeeding with CO. (Bottom) Propanal selectivity of tandem hydroformylation. (C) Cofeeding with H_2 and (D) cofeeding with CO.

Table 1. Tandem Hydroformylation of Different Alkenes

reaction conditions[a]		aldehyde selectivity (%)	
alkene	temperature (°C)	tandem hydroformylation	single-step hydroformylation
ethylene	150	48.9	2.2
propylene	190	47.7	1.3
1-butene	230	48.2	0.9

[a]Tandem alkene hydroformylation: 35 Torr of methanol, 7.5 Torr of alkene, and 727.5 Torr of helium. Single-step hydroformylation with CO and H_2: 35 Torr of CO, 70 Torr of H_2, 7.5 Torr of alkene, and 657.5 Torr of helium.

formylation reaction where propylene and 1-butene were reacted with CO and H_2.

2.2.5. Proposed Reaction Mechanism. Combining the insights provided by preceding results, we proposed a mechanism for the tandem reaction with methanol and ethylene catalyzed by CeO_2−Pt@mSiO_2 (Figure 7). In this proposed mechanism, ethylene molecules are adsorbed on the platinum surface and occupy the majority of active sites, hindering the dissociation of methanol on the Pt/CeO_2 interface. At limited active sites, methanol molecules will dissociate to form hydrogen species (H_{ads}) and intermediate products (e.g., CH_3O*, CH_2O*, CHO*, hereafter abbreviated as "CHO_{ads} species") in microscopic amounts,[23,25−28] which are adsorbed on the surface. The presence of these "CHO_{ads} species" in methanol decomposition has long been known.[25−37] Both experimental and theoretical studies have found that the methanol decomposition on platinum surface proceeds via methoxy (CH_3O), as a first intermediate, then by stepwise hydrogen abstraction via formaldehyde (CH_2O), and then formyl (CHO). The formation of these intermediates from methanol on the Pt surface has been detected by energy electron loss spectroscopy (EELS),[30−33,37] thermal desorption spectroscopy (TDS),[29−33,35,36] low-energy electron diffraction

Figure 7. Proposed reaction pathway for the tandem ethylene hydroformylation.

(LEED),[30,37] infrared reflection−absorption spectroscopy (IRAS),[34] and X-ray photoelectron spectroscopy.[25,37] In our proposed tandem reaction pathway, the ratio of the H_{ads} and CHO_{ads} intermediates could be determined from the methanol decomposition stoichiometry. These adsorbed intermediates then diffuse from the Pt/CeO_2 interface to the nearby Pt/SiO_2 interface, where they are consumed by adsorbed ethylene. The ethylene then reacts with these CHO_{ads} species to generate propanal or with H_{ads} to produce ethane as a byproduct.[12] At low temperatures, the CHO_{ads} and H_{ads} species are produced in very small amounts, and thus the adsorbed ethylene molecules are in great excess. Consequently, we can assume each CHO_{ads} species and H_{ads} are consumed by the adsorbed ethylene and do not accumulate on the platinum surface, resulting in a propanal selectivity of ~50%. With elevated temperatures, the

DOI: 10.1021/jacs.6b03915
J. Am. Chem. Soc. 2016, 138, 11568−11574

coverage of CHO_{ads} and H_{ads} on the Pt surface increases along with the methanol decomposition rate, thereby increasing the opportunity for reactions between ethylene and both H_{ads} and the CHO_{ads} species. Thus, the reaction rates for hydroformylation and hydrogenation should both increase, which is consistent with our results. However, as the amounts of CHO_{ads} and H_{ads} increase, it is no longer valid to assume that they are consumed immediately by ethylene, and they likely begin to accumulate on the Pt surface. Considering that ethylene hydrogenation is faster than hydroformylation, the overall hydrogenation rate is higher than that of hydroformylation, which is responsible for the decline of propanal selectivity. However, in the case of the single-step hydroformylation, the reaction pathway is different. Macroscopic CO and H_2 are introduced to the catalyst and adsorbed on the Pt surface, which leads to an inevitable accumulation of H_{ads}. As the ethylene hydrogenation is more favorable than the ethylene hydroformylation reaction, ethane will always be the dominant product.

3. CONCLUSION

A stable 3D tandem catalyst CeO_2−Pt@$mSiO_2$ with well-defined catalytic interfaces was developed, and its catalytic performance was studied in tandem alkene hydroformylation with methanol. Importantly, the tandem ethylene hydroformylation exhibited greatly enhanced propanal selectivity compared to the single-step ethylene hydroformylation with CO and H_2, which could further be improved by cofeeding with CO. This effective production of propanal results from synergy between the two sequential chemical conversions facilitated by CeO_2−Pt@$mSiO_2$ and the altered reaction pathway, compared to the single-step reaction. Ultimately, this in-depth study highlights the benefits of tandem catalysis and paves the way for further rational design of complex nanostructured catalysts.

EXPERIMENTAL METHODS

Chemicals. Cerium nitrate hexahydrate (99% trace metals basis), poly(vinylpyrrolidone) (PVP, M_w = 360,000), PVP (M_w = 29000), tetradecyltrimethylammonium bromide (TTAB), cetrimonium bromide (CTAB) (99%), and tetraethyl orthosilicate (TEOS) (99.999% trace metal basis) were purchased from Sigma-Aldrich. Ammonium hexachloroplatinate (IV) [$(NH_4)_2PtCl_6$, Pt 43.4% min] was purchased from Alfa Aesar. Ethanol and ethylene glycol were purchased from Fisher Chemical. Ammonia solution (28−30%) was purchased from EMD Millipore. All chemicals were used as received without further purification.

Synthesis of CeO_2 Nanoparticles. Cerium nitrate hexahydrate (0.85 g) was dissolved in a mixture of deionized water (5 mL) and ethanol (5 mL). To this solution was added 30 mL of a PVP (M_w = 360000) ethanol solution (60 mg/mL). This reaction mixture was heated in a stainless-steel autoclave to 140 °C for 24 h. The as-synthesized CeO_2 nanoparticles were collected by centrifugation (12000 rpm, 60 min) and then washed twice with water and ethanol and stored in ethanol for further synthesis.

Overgrowth of Pt NPs on As-Synthesized CeO_2 NPs. The as-synthesized CeO_2 nanoparticles (40 mg) were dispersed in 20 mL ethanol. TTAB (36.8 mg) and PVP (M_w = 29000, 21.8 mg) dissolved in ethylene glycol (16 mL) were added to the CeO_2 NPs/ethanol solution. $(NH_4)_2Pt(IV)Cl_6$ (9.75 mg, this amount can be changed accordingly to tune the Pt loading amount) was dissolved into ethylene glycol (4 mL) in a 25 mL three-neck round flask at 80 °C under argon protection with magnetic stirring. This Pt precursor solution was mixed with the CeO_2 NPs/ethanol solution and heated to 140 °C for 6 h in a stainless-steel autoclave. The as-synthesized CeO_2−Pt NPs were separated by centrifugation (12000 rpm, 45 min) and then redispersed in 40 mL deionized water.

Synthesis of CeO_2−Pt@$mSiO_2$ Tandem Catalyst. The CeO_2−Pt@$mSiO_2$ core−shell nanoparticles were prepared by a reported sol−gel method with some modification. The solution of presynthesized CeO_2−Pt (40 mg in 45 mL deionized water) was mixed with a solution of CTAB, which was prepared by dissolving 225 mg CTAB in 30 mL of ethanol. An ammonia solution (0.2 mL) was added to the above solution with stirring. A controlled amount of 1 vol % TEOS diluted with ethanol was then added under continuous magnetic stirring at room temperature. After 6 h, the as-synthesized CeO_2−Pt@SiO_2 nanoparticles were obtained by centrifugation (6000 rpm, 5 min). The product was calcined at 350 °C for 1 h in static air to remove the CTAB template and other surfactants (PVP, TTAB) to generate CeO_2−Pt@$mSiO_2$ particles with clean interfaces.

Characterization of CeO_2−Pt@$mSiO_2$ Tandem Catalyst. The structural analysis of the composite nanoparticles was performed using transmission electron microscopy (TEM) on a FEI Tecnai F20 at an accelerating voltage of 200 kV. High-angle annular dark-field scanning transmission electron microscopy (HAADF-STEM) and energy-dispersive X-ray spectroscopy (EDS) mapping was carried out with an FEI TitanX 60−300, which provided the elemental distribution of the catalyst. The surface area and pore size distribution of the catalyst were obtained by nitrogen physisorption experiments, which were carried out on a Quantachrome Autosorb-1 analyzer. Platinum quantitative analysis by inductively coupled plasma atomic emission spectroscopy (ICP-AES) was carried out on a PerkinElmer optical emission spectrometer (Optima 7000 DV). Before the ICP-AES measurement, the catalyst was digested in aqua regia for 24 h, and then deionized water was added to dilute the solution. A clear solution was obtained for the ICP-AES measurement by centrifuging at 4000 rpm to remove sediment.

Catalytic Reactions. The reactions were carried out in a batch-mode reactor equipped with a boron nitride substrate heater and a metal bellows circulation pump for gas mixing (Section S2 and Figure S1). For the alkene hydroformylation with CO and H_2 formed by methanol decomposition, the reactor was typically filled with 35 Torr of methanol, 7.5 Torr of alkene, and 727.5 Torr of helium. For single-step alkene hydroformylation, the reactor was typically filled with 35 Torr of CO, 70 Torr of H_2, 7.5 Torr of alkene, and 657.5 Torr of helium.

The products were analyzed approximately every 20 min by a gas chromatograph (GC) equipped with both a flame ionization detector (FID) and a thermal conductivity detector (TCD). The carrier gas was helium, the FID was used to quantify the alkene and aldehyde products, and the TCD was used for CO quantification.

The turnover frequency values are derived by the number of Pt active sites, and the number of propanal molecules produced as monitored by GC. The TOF was calculated based on the experiment data with a conversion of reactants below 20% (Section S2). The propanal selectivity was calculated on a carbon basis and defined as follows:

$$\text{propanal selectivity} = (\text{propanal formed})/(\text{ethylene converted}) \times 100\%$$

ASSOCIATED CONTENT

Supporting Information

The Supporting Information is available free of charge on the ACS Publications website at DOI: 10.1021/jacs.6b03915.

Additional synthesis details, BET characterization, additional TEM images, and catalytic performance of catalyst (PDF)

AUTHOR INFORMATION

Corresponding Authors

*somorjai@berkeley.edu

DOI: 10.1021/jacs.6b03915
J. Am. Chem. Soc. 2016, 138, 11568−11574

*p_yang@berkeley.edu

Present Address

[‖]C.C.: Department of Chemistry, Tsinghua University, Beijing 100084, P. R. China.

Author Contributions

[⊥]J.S., C.X., and C.C. contributed equally to this work.

Notes

The authors declare no competing financial interest.

■ ACKNOWLEDGMENTS

This work was supported by the Office of Basic Energy Sciences (BES), Division of Materials Sciences and Engineering, of the U.S. Department of Energy (DOE) under Contract DE-AC02-05CH11231, through the Chemical and Mechanical Properties of Surfaces, Interfaces and Nanostructures program (FWP KC3101). Work at the Molecular Foundry was supported by the Office of Science, Office of Basic Energy Sciences, of the U.S. Department of Energy under Contract DE-AC02-05CH11231. We acknowledge Dr. Gerome Melaet and Mr. Walter Ralston for the help with catalytic reactions. C.X. acknowledges support from Suzhou Industrial Park fellowship. Dr. Katie R. Meihaus is acknowledged for editorial assistance.

■ REFERENCES

(1) Studt, F.; Sharafutdinov, I.; Abild-Pedersen, F.; Elkjaer, C. F.; Hummelshoj, J. S.; Dahl, S.; Chorkendorff, I.; Norskov, J. K. *Nat. Chem.* **2014**, *6*, 320.
(2) Behrens, M.; Studt, F.; Kasatkin, I.; Kuhl, S.; Havecker, M.; Abild-Pedersen, F.; Zander, S.; Girgsdies, F.; Kurr, P.; Kniep, B. L.; Tovar, M.; Fischer, R. W.; Norskov, J. K.; Schlogl, R. *Science* **2012**, *336*, 893.
(3) Jiao, F.; Li, J.; Pan, X.; Xiao, J.; Li, H.; Ma, H.; Wei, M.; Pan, Y.; Zhou, Z.; Li, M.; Miao, S.; Li, J.; Zhu, Y.; Xiao, D.; He, T.; Yang, J.; Qi, F.; Fu, Q.; Bao, X. *Science* **2016**, *351*, 1065.
(4) An, K.; Alayoglu, S.; Musselwhite, N.; Plamthottam, S.; Melaet, G.; Lindeman, A. E.; Somorjai, G. A. *J. Am. Chem. Soc.* **2013**, *135*, 16689.
(5) Schwab, G. M.; Koller, K. *J. Am. Chem. Soc.* **1968**, *90*, 3078.
(6) Fu, Q.; Saltsburg, H.; Flytzani-Stephanopoulos, M. *Science* **2003**, *301*, 935.
(7) Chen, G.; Zhao, Y.; Fu, G.; Duchesne, P. N.; Gu, L.; Zheng, Y.; Weng, X.; Chen, M.; Zhang, P.; Pao, C.-W.; Lee, J.-F.; Zheng, N. *Science* **2014**, *344*, 495.
(8) Cargnello, M.; Doan-Nguyen, V. V. T.; Gordon, T. R.; Diaz, R. E.; Stach, E. A.; Gorte, R. J.; Fornasiero, P.; Murray, C. B. *Science* **2013**, *341*, 771.
(9) Yamada, Y.; Tsung, C.-K.; Huang, W.; Huo, Z.; Habas, S. E.; Soejima, T.; Aliaga, C. E.; Somorjai, G. A.; Yang, P. *Nat. Chem.* **2011**, *3*, 372.
(10) Ojima, I.; Tsai, C.-Y.; Tzamarioudaki, M.; Bonafoux, D. *Organic Reactions*; John Wiley & Sons, Inc., 2004.
(11) Dharmidhikari, S.; Abraham, M. A. *J. Supercrit. Fluids* **2000**, *18*, 1.
(12) Naito, S.; Tanimoto, M. *J. Chem. Soc., Chem. Commun.* **1989**, 1403.
(13) Hanaoka, T.; Arakawa, H.; Matsuzaki, T.; Sugi, Y.; Kanno, K.; Abe, Y. *Catal. Today* **2000**, *58*, 271.
(14) Gao, R.; Tan, C. D.; Baker, R. T. K. *Catal. Today* **2001**, *65*, 19.
(15) Takahashi, N.; Kobayashi, M. *J. Catal.* **1984**, *85*, 89.
(16) Arai, H.; Tominaga, H. *J. Catal.* **1982**, *75*, 188.
(17) Rioux, R. M.; Song, H.; Hoefelmeyer, J. D.; Yang, P.; Somorjai, G. A. *J. Phys. Chem. B* **2005**, *109*, 2192.
(18) Song, H.; Rioux, R. M.; Hoefelmeyer, J. D.; Komor, R.; Niesz, K.; Grass, M.; Yang, P.; Somorjai, G. A. *J. Am. Chem. Soc.* **2006**, *128*, 3027.
(19) Tsung, C.-K.; Kuhn, J. N.; Huang, W.; Aliaga, C.; Hung, L.-I.; Somorjai, G. A.; Yang, P. *J. Am. Chem. Soc.* **2009**, *131*, 5816.
(20) Somorjai, G. A.; Frei, H.; Park, J. Y. *J. Am. Chem. Soc.* **2009**, *131*, 16589.
(21) Joo, S. H.; Park, J. Y.; Tsung, C.-K.; Yamada, Y.; Yang, P.; Somorjai, G. A. *Nat. Mater.* **2009**, *8*, 126.
(22) Croy, J. R.; Mostafa, S.; Liu, J.; Sohn, Y.; Heinrich, H.; Cuenya, B. R. *Catal. Lett.* **2007**, *119*, 209.
(23) Imamura, S.; Higashihara, T.; Saito, Y.; Aritani, H.; Kanai, H.; Matsumura, Y.; Tsuda, N. *Catal. Today* **1999**, *50*, 369.
(24) Deng, Y.; Qi, D.; Deng, C.; Zhang, X.; Zhao, D. *J. Am. Chem. Soc.* **2008**, *130*, 28.
(25) Matolín, V.; Johánek, V.; Škoda, M.; Tsud, N.; Prince, K. C.; Skála, T.; Matolínová, I. *Langmuir* **2010**, *26*, 13333.
(26) Cao, D.; Lu, G. Q.; Wieckowski, A.; Wasileski, S. A.; Neurock, M. *J. Phys. Chem. B* **2005**, *109*, 11622.
(27) Greeley, J.; Mavrikakis, M. *J. Am. Chem. Soc.* **2002**, *124*, 7193.
(28) Greeley, J.; Mavrikakis, M. *J. Am. Chem. Soc.* **2004**, *126*, 3910.
(29) Waszczuk, P.; Lu, G. Q.; Wieckowski, A.; Lu, C.; Rice, C.; Masel, R. I. *Electrochim. Acta* **2002**, *47*, 3637.
(30) Wang, J.; Masel, R. I. *J. Vac. Sci. Technol., A* **1991**, *9*, 1879.
(31) Franaszczuk, K.; Herrero, E.; Zelenay, P.; Wieckowski, A.; Wang, J.; Masel, R. I. *J. Phys. Chem.* **1992**, *96*, 8509.
(32) Diekhöner, L.; Butler, D. A.; Baurichter, A.; Luntz, A. C. *Surf. Sci.* **1998**, *409*, 384.
(33) Wang, J.; Masel, R. I. *Surf. Sci.* **1991**, *243*, 199.
(34) Peremans, A.; Maseri, F.; Darville, J.; Gilles, J. M. *Surf. Sci.* **1990**, *227*, 73.
(35) Davis, J. L.; Barteau, M. A. *Surf. Sci.* **1987**, *187*, 387.
(36) Akhter, S.; White, J. M. *Surf. Sci.* **1986**, *167*, 101.
(37) Attard, G. A.; Chibane, K.; Ebert, H. D.; Parsons, R. *Surf. Sci.* **1989**, *224*, 311.

DOI: 10.1021/jacs.6b03915
J. Am. Chem. Soc. 2016, 138, 11568−11574